Effects of Relativity on Quadrupole Oscillations of Compact Stars

Abhijit Gupta

North Carolina School of Science and Mathematics, 1219 Broad Street Durham, North Carolina 27705

Mentorship from Jonathan Bennett (NCSSM), Charles R. Evans and S. Reece Boston (UNC-Chapel Hill)

Abstract

In the present age of space-based photometry, telescopes such as K2 and TESS are providing pulsation frequencies of stellar objects to unprecedented accuracy, requiring equally precise theoretical models correlating these observations to mass- and composition-dependent characteristics of stars. At this precision, relativistic models are required for compact objects such as white dwarfs and neutron stars. I model these stars as polytropes using the Tolman-Oppenheimer-Volkoff equation, and compute relativistic nonradial stellar pulsations around this equilibrium state. Outside the stellar surface, I integrate the Zerilli equation to locate resonant quasinormal modes, where ingoing gravitational radiation vanishes. I compare the frequencies of a subset of these modes to their corresponding pressure-modes in the Newtonian limit, as a function of the strength of relativity inside the star. Our results contribute to our understanding of the impact of general relativity on stellar oscillations, and can be used to determine the conditions under which the Newtonian approximation is justified.

Contents

1 Motivation

1.1 Asteroseismology

Although stars generally evolve on extremely long timescales, they are not static but pulsate periodically around an equilibrium. The frequencies of these oscillations inform us about internal characteristics of the star, such as mass, radius, pressure, and density. While these variables cannot be directly measured, telescopes can detect luminosity deviations that stellar pulsation cause. The frequencies of these oscillations are the frequencies of the stellar pulsations.

Asteroseismology, the study of these stellar pulsations, involves two components: theoretical calculations and experimental observations. Theoretical programs assume a particular equilibrium state, and then model perturbations on this system. Only pulsations which satisfy boundary conditions at both the interior and stellar surface can possibly occur. Each pulsation can be described by a frequency and spherical harmonic degree and mode. The experimental observations measure periodic luminosity oscillations of stars over long periods of time. A Fourier transform is performed, and after filtering, spikes in the frequency curve are used to determine potential eigenfrequencies.

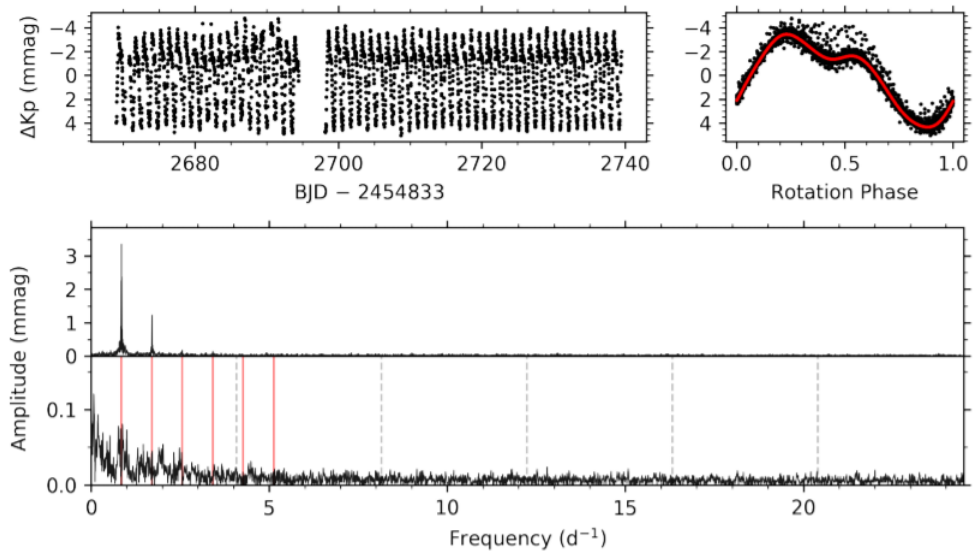

Figure 1: Experimental results from the K2 mission. The top panels show the standard and phase-folded light curves. The bottom panel shows the amplitude and residual amplitude spectrum after the pulsation frequencies are removed . Red vertical lines indicate observed pulsation frequencies [1]

Given these experimentally determined frequencies, programs can be run to determine the predicted central density, central pressure, total mass, radius, and many additional stellar variables. Asteroseismology presents an additional method to calculating these variables, alongside existing procedures. The combination yields stronger approximations than any method individually.

1.2 Compact Objects

In recent years, space-based telescopes such as NASA's Kepler spacecraft and Transiting Exoplanet Survey Satellite (TESS) are providing pulsation frequencies of stellar objects with unprecedented accuracy. Equally precise theoretical models correlating these observations to mass- and composition-dependent characteristics of stars is required to make full use of these satellites. Present theoretical models have reduced error to less than 1 part in 10^7, roughly equivalent to the observational accuracy of these telescopes [2]. However, when studying highly-dense compact objects, general relativity can have a noticeable impact on the stellar structure and pulsations, requiring more rigorous models.

While most stars are not substantially affected by general relativity, a class of compact objects require general relativistic corrections to accurately model the pulsations to the desired accuracy due to their extreme densities. Among compact objects, there are two main classes of stars: white dwarf and neutron stars. White dwarfs are the remnants of low-mass to medium-mass stars that have exhausted their hydrogen and helium supplies. These stars are composed of heavier elements such as carbon and oxygen, and support themselves against gravitational collapse with electron degeneracy pressure. The density of a white dwarf is some 10^6 times greater than that of our Sun.

Even more extreme are neutron stars, formed by the supernova explosions of stars not quite large enough to produce black holes. Neutron stars are similar to white dwarfs except are composed almost entirely of neutrons and supported with neutron degeneracy pressure instead of electron degeneracy. Physicists are still unsure exactly what types of matter are present at the very center of a neutron star, where density is the highest. Neutron stars are believed to be the densest macroscopic objects in the Universe, with densities about 10^{15} times higher than that of the Sun.

Relativistic corrections have small but noticeable impacts on white dwarfs, but are essential to study the pulsation frequencies of neutron stars. By better understanding the pulsations of neutron stars, we gain a better understanding of its interior. Physicists are still unsure of the state of matter and characteristics of the neutron star core, given its extreme density. Recent research even suggests that the matter in a neutron star may be the strongest material in the Universe, 10 billion times stronger than steel [3]. Relativistic asteroseismology can assist in evaluating the different models attempting to describe the neutron star interior by providing accurate experimental data on neutron star properties.

In this paper, I analyze how general relativity impacts the stellar pulsations of compact objects. By understanding when the Newtonian approximation is justified for a given error tolerance, we can improve the computational efficiency of theoretical asteroseismology without decreasing accuracy. On the contrary, computational improvements to previously published algorithms make our results potentially more accurate than existing results. Additionally, this research has applications to understanding the yet unknown physics governing the dense neutron star cores.

2 Stellar Equilibrium

The radius-dependent characteristics of compact objects affect their stellar pulsations, so an accurate model of the equilibrium state is required before computing stellar pulsation eigenfrequencies and other characteristics. To simplify calculations, a polytropic model is used in both the Newtonian and relativistic calculations [4]. A polytrope is a star where pressure (p) and density (ρ) are continuous with respect to radius, and are related by the equation of state:

$$p = \kappa\rho^{(n+1)/n} \tag{1}$$

where κ is the constant of proportionality, and n is the polytropic index. A polytropic index between 0.5 and 1 generally models a neutron star well, while white dwarfs are modeled with a polytropic index of 3.

2.1 Newtonian Equilibrium

In flat spacetime, the Lane-Emden equation describes the relationship between radius and density for polytropic stars, derived from the equation of hydrostatic equilibrium and the mass-continuity equation [4].

$$\frac{1}{\xi^2}\frac{d}{d\xi}\left(\xi^2\frac{d\theta}{d\xi}\right) + \theta^n = 0 \tag{2}$$

where θ is defined by $\rho = \rho_c\theta^n$, ρ_c being the central density. ξ is the dimensionless radius defined by:

$$\xi = R\sqrt{\frac{4\pi G}{(n+1)\kappa\rho_c^{\frac{1}{n}-1}}} \tag{3}$$

where G is the universal gravitation constant. The boundary conditions for this differential equation are $\theta(0) = 1$ and $\theta'(0) = 0$. The first equation represents mass conservation, and the second equation represents hydrostatic equilibrium. For $n = 0$, $n = 1$, and $n = 5$, analytic solutions are available. For any other polytropic index, numerical integration to $\theta = 0$ is required to analyze the equilibrium conditions of the star. Specifically, the Lane-Emden equation can be separated into two coupled first-order ODEs using:

$$\frac{d\theta}{d\xi} = -\frac{\psi}{\xi^2} \tag{4}$$

$$\frac{d\psi}{d\xi} = \theta^n\xi^2 \tag{5}$$

Adaptive step-size fourth-order Runge-Kutta numerical integration is run on the system until the first step where $\theta < 0$. Newton's Method is used to locate ξ where $\theta = 0$. At this point, pressure and density become 0, marking the outer edge of the star. Figure 2 shows θ vs. ξ for varying polytropic index n.

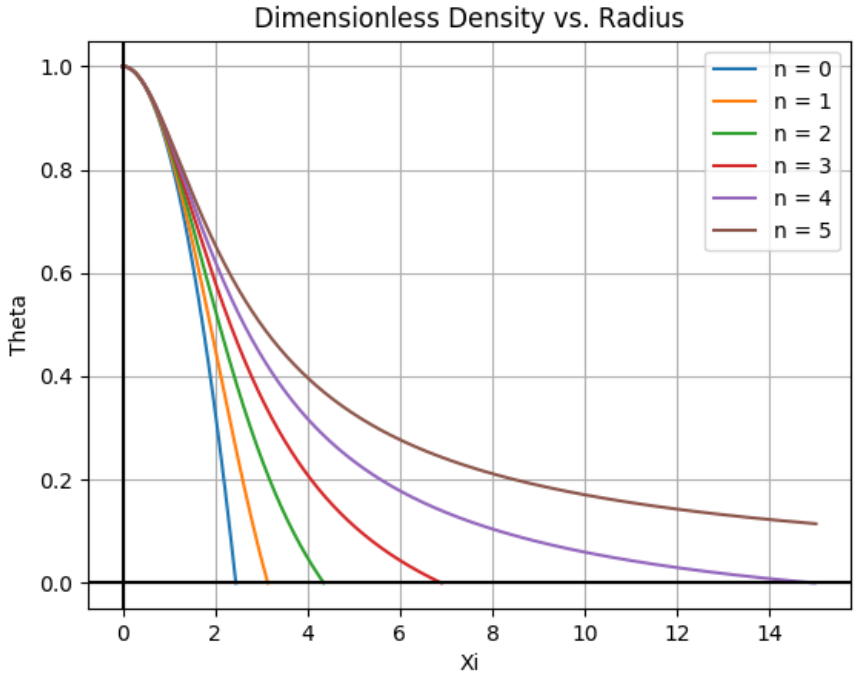

Figure 2: θ vs. ξ for varying n. $n = 0$ has θ decline the fastest, while $n = 5$ decreases asymptotically but never reaches $\theta = 0$. Neutron stars have $n \approx 1$, and white dwarfs have $n \approx 3$

2.2 Relativistic Equilibrium

While the Newtonian model is accurate in predicting the oscillation frequencies of main sequence stars, general relativity is needed to accurately describe compact objects with immense densities. The quantity σ approximates how relativistic a star is:

$$\sigma = \frac{p_c}{\rho_c} = \kappa \rho_c^{1/n} \tag{6}$$

The greater σ, the greater the impacts of general relativity on both the equilibrium and stellar oscillations. For a white dwarf star, $\sigma \approx 0.001$, while for a neutron star, $\sigma \approx 0.1$. In this paper, I shall consider all stars in Schwarzschild spacetime, where spherical symmetry is assumed and there is no stellar rotation or magnetism involved [5]. The Schwarzschild metric tensor describes the spacetime:

$$g_{uv} = \begin{pmatrix} -e^{\nu} & 0 & 0 & 0 \\ 0 & e^{\lambda} & 0 & 0 \\ 0 & 0 & r^2 & 0 \\ 0 & 0 & 0 & r^2 \sin^2(\theta) \end{pmatrix} \tag{7}$$

where $e^{-\lambda(r)} = 1 - 2M(r)/r$. e^{ν} relates to the mass of the star, but cannot be analytically represented for a relativistic polytropic star. Equation (7) is given in geometric units ($c = 1$, $G = 1$), in standard

Schwarzschild coordinates (t, r, θ, ϕ).

A relativistic equivalent of the Lane-Emden equation, the Tolman-Oppenheimer-Volkoff (TOV) Equation, takes into account curved spacetime in describing polytropic stars. It calculates P, ρ, and ν as a function of radius. The TOV Equation can be written as three coupled first-order ODEs [6].

$$\frac{dM}{dr} = 4\pi r^2 \rho \qquad (8) \qquad \frac{d\nu}{dr} = 2\frac{M + 4\pi r^3 p}{r(r - 2M)} \qquad (9) \qquad \frac{dp}{dr} = -\frac{1}{2}(\rho + p)\frac{d\nu}{dr} \qquad (10)$$

With boundary conditions $M(0) = 0$, $\nu(R) = 1 - 2M/R$, and $p(0) = p_0$, I solve this system very similarly to the Lane-Emden equation. The numerical results of the equilibrium analysis, radius-dependent p, ρ, ν, λ, and M, are used when analyzing the stellar pulsations.

2.3 Comparison

The below figure compares the results of the Lane-Emden Equation and TOV Equation for a neutron star with typical characteristics. While the shape of the curves are similar, there is a noticeable difference in radius and mass (integral of density vs. radius).

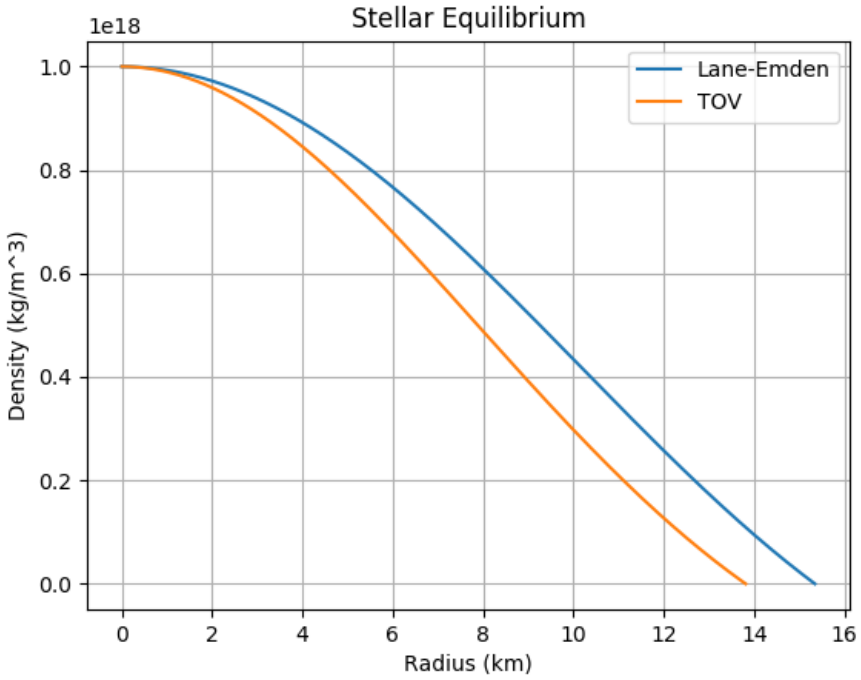

Figure 3: Comparison of solutions to Lane-Emden Equation and TOV Equation for neutron star with polytropic index $n = 1$. The TOV Equation predicts smaller radius and mass.

The TOV Equation is used in all relativistic stellar pulsation calculations as the equilibrium model. Relativistic effects can be attributed both to differences in the equations governing stellar equilibrium, and differences in the equations governing stellar pulsations.

3 Stellar Pulsations

To analyze stellar pulsations, a perturbation is applied and propagated through the polytropic equilibrium state. Only under certain eigenfrequencies will the solution be continuous throughout the star. These oscillations can be both radial or nonradial, and each have a spherical harmonic degree l and mode m.

Furthermore, the oscillations can be grouped into families of modes, depending on their restoring forces. The two most important classifications are Pressure modes (p-modes) and Gravity modes (g-modes). P-modes are high frequency modes whose deviations from equilibrium are counteracted by pressure changes in the convective zone. G-modes are low frequency modes, counteracted by mass movement in the radiative zone. In this research, I focus on p-modes, although our methods apply to g-modes as well.

For a specific spherical harmonic degree, spherical harmonic mode, and mode classification, there are multiple energy eigenmodes with ascending mode number k. The three variables, l, m, and k, along with the mode classification, fully describe a particular stellar pulsation.

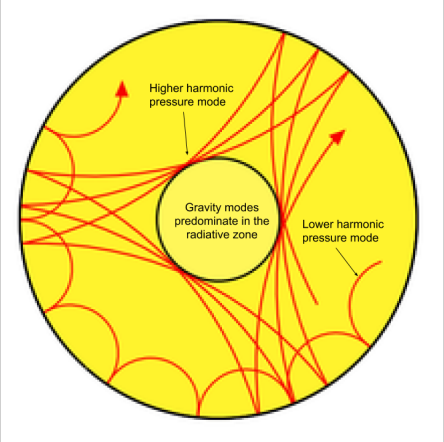

Figure 4: P-mode propagation for two distinct harmonics. The number of reflections is the degree. The resonant modes result from a superposition of component waves travelling in opposite directions [7]

These stellar pulsations have separable time, angle, and radius dependence, given by:

$$f(t,r,\theta,\phi) = \sum_{l=0}^{l=\infty} \sum_{m=-l}^{l} f_l(r) r^l Y_l^m(\theta,\phi) e^{-i\omega t} \tag{11}$$

$$Y_l^m(\theta,\phi) = N e^{im\phi} P_l^m(cos\theta) \tag{12}$$

where $f(t,r,\theta,\phi)$ is a perturbation function, ω is the frequency, $P_l^m(\cos\theta)$ is the associated Legendre polynomial, and N is a normalizing factor. Now, by calculating $f_l(r)$, the radial-dependent perturbation for a specific eigenfrequency, the overall nature of the oscillations can be understood. While all degrees from 0 to ∞ could occur, in reality only the first few have substantial amplitude. $l = 2$ is the first degree at which gravitational radiation occurs in the relativistic model, making it the most optimal case-study.

4 Newtonian Quadrupole Oscillations

4.1 Pulsations Inside the Star

In Newtonian spacetime, a set of four homogeneous first-order differential equations describe the perturbations of radial displacement, pressure, gravitational potential, and gravitational acceleration. Physically, these relations are derived by maintaining continuous variables and appropriate boundary conditions.

The system of differential equations originally is dimensioned, but can be made dimensionless, with perturbation variables y_1 through y_4 representing fractional changes in radius, pressure, gravitational potential, and gravitational acceleration. The solutions to the system are independent of all stellar equilibrium factors, except the polytropic index, allowing this dimensionless analysis. The differential equations for these variables can be written as one matrix equation [8].

$$\frac{d}{dx}\begin{bmatrix} y_{1,l} \\ y_{2,l} \\ y_{3,l} \\ y_{4,l} \end{bmatrix} = \frac{1}{x}\begin{bmatrix} V_g - 3 & \frac{l(l+1)}{c_1\omega^2} - V_g & V_g & 0 \\ c_1\omega^2 - A_* & A_* - U + 1 & -A_* & 0 \\ 0 & 0 & 1 - U & 1 \\ UA_* & UV_g & l(l+1) - UV_g & -U \end{bmatrix}\begin{bmatrix} y_{1,l} \\ y_{2,l} \\ y_{3,l} \\ y_{4,l} \end{bmatrix} \tag{13}$$

The $1/x$ term in front of the matrix causes potential singularities in the integration, and also requires further emphasis closer to $x = 0$, where the system changes faster. To improve computational accuracy, I apply a change of variables from x to $\ln(x)$, yielding this simpler form:

$$\frac{d}{d\ln(x)}\begin{bmatrix} y_{1,l} \\ y_{2,l} \\ y_{3,l} \\ y_{4,l} \end{bmatrix} = \begin{bmatrix} V_g - 3 & \frac{l(l+1)}{c_1\omega^2} - V_g & V_g & 0 \\ c_1\omega^2 - A_* & A_* - U + 1 & -A_* & 0 \\ 0 & 0 & 1 - U & 1 \\ UA_* & UV_g & l(l+1) - UV_g & -U \end{bmatrix}\begin{bmatrix} y_{1,l} \\ y_{2,l} \\ y_{3,l} \\ y_{4,l} \end{bmatrix} \tag{14}$$

A_*, U, V_g, and c_1 are dimensionless stellar equilibrium quantities as defined in [8]. Although they contain ρ and p, all can be simplified to dimensionless form using ξ and θ. A_* is the Eulerian pressure perturbation, c_1 is an inverse scaled average density, and U and V_g are common stellar variables.

$$A_* = -r\left(\frac{\nabla\rho_c}{\rho_c} - \frac{n\nabla p_c}{(n+1)p_c}\right) = -r\left(\frac{1}{\rho}\frac{d\rho_c}{dr} - \frac{n}{(n+1)p}\frac{dp_c}{dr}\right) \tag{15}$$

$$U = \frac{d\ln m(r)}{d\ln r} = \frac{4\pi G\rho r}{g} \tag{16}$$

$$V_g = -\frac{n}{n+1}\frac{d\ln p}{d\ln r} = \frac{gr\rho n}{p(n+1)} \tag{17}$$

$$c_1 = \left(\frac{M}{m(r)}\right)\left(\frac{r}{R}\right)^3 \tag{18}$$

x is the dimensionless radius, ranging from 0 to 1. ω refers to the frequency of the oscillation being tested, and is made dimensionless by multiplying the dimensioned frequency by $\sqrt{R^3/GM}$. ρ_c and p_c are the central density and pressure, respectively.

The system of differential equations has central and surface boundary conditions, defined below. These conditions ensure the solution is physically acceptable at both boundaries [8].

$$\text{Central BCs} = \begin{cases} y_1 = l * U_0 \\ y_2 = c_1(0)\omega^2 * U_0 \\ y_3 = Y_0 \\ y_4 = l * Y_0 \end{cases} \tag{19}$$

$$\text{Surface BCs} = \begin{cases} y_1 = 1 \\ y_2 = 1 + Y_S \\ y_3 = Y_S \\ y_4 = -(l+1) * Y_S \end{cases} \tag{20}$$

The differential equations are singular at both boundaries due to division by zero-valued variables. At the center of the star ($x = 0$), $\ln(x)$ is not defined, and at the outer surface of the star ($x = 1$), pressure is zero and V_g and A_* approach ∞. To handle this issue, I use the Magnus Multiple Shooting Scheme [9]. Two arbitrary solutions satisfying the boundary conditions are created on both boundaries, and integrated to $x = 0.5$. They are inserted into a matrix, and the determinant is computed. Eigenfrequencies are found when the determinant of this square matrix is 0. Adaptive steps-size fourth-order Runge-Kutta integration is used to integrate the system, and Newton's Method is used during root-finding to locate where $\det(M) = 0$ with quadratic convergence.

4.2 Algorithmic Roadmap

In this section, I explain the specific steps taken to accurately compute the resonant modes of Newtonian polytropic stars. The code used to implement this algorithm was written in Python 3.

1. The central pressure and density of the star are provided. The polytropic index n is given as well. From these, fourth-order Runge-Kutta integration is used on the Lane-Emden Equation (Eq. 2).

2. For a test frequency and spherical harmonic degree, the perturbation variables are calculated at both boundaries using boundary conditions (Eq. 19-20). Two possible solutions on each end are integrated to $r = 0.5R$ using fourth-order Runge-Kutta integration (Eq. 14). The equations are treated in matrix form for improved computational efficiency.

3. Using the Magnus Multiple Shooting Scheme, the determinant of a $4x4$ square matrix of partial solutions is calculated. Each row is a single integration from the previous step, and all four solutions are used. A determinant of 0 corresponds to an eigenfrequency.

4. Steps 2 and 3 are repeated keeping the spherical harmonic degree constant and varying the test frequency. Newton's Method is used to locate where $\det(M) = 0$ with quadratic convergence. The derivative required for Newton's Method is approximated by sampling two points slightly above and below the test frequency. Newton's Method is run until a certain threshold accuracy is obtained.

5. Steps 2 to 5 are repeated for each spherical harmonic degree. In this paper, results for $l = 2$ are shown, although others can be calculated with this algorithm. $l = 2$ is of particular importance because it accounts for the majority of gravitational radiation in the relativistic system.

5 Newtonian Model Results and Discussion

The figure below shows the normalized perturbations of a polytrope with index $n = 3$ as a function of dimensionless radius x. Although $n = 3$ best represents a white dwarf, a neutron star's pulsations could be seen with $n = 1$. I use $n = 3$ for ease of comparison to prior calculations for main-sequence stars, also well approximated with $n = 3$. The spherical harmonic is $l = 2$, and this particular perturbation is the second-harmonic pressure-mode. I refer to the fundamental or lowest frequency mode in a family as the first-harmonic. $l = 2$ is chosen because it is the lowest spherical harmonic degree for which gravitational waves occur in the relativistic model.

The four graphs left to right and top to bottom are radial perturbation, pressure perturbation, gravitational potential perturbation, and gravitational field perturbation, y_1 to y_4 in the above calculations. Radial displacement and pressure perturbations are largest near the center of the star, and all four perturbation variables approach zero near the surface of the star.

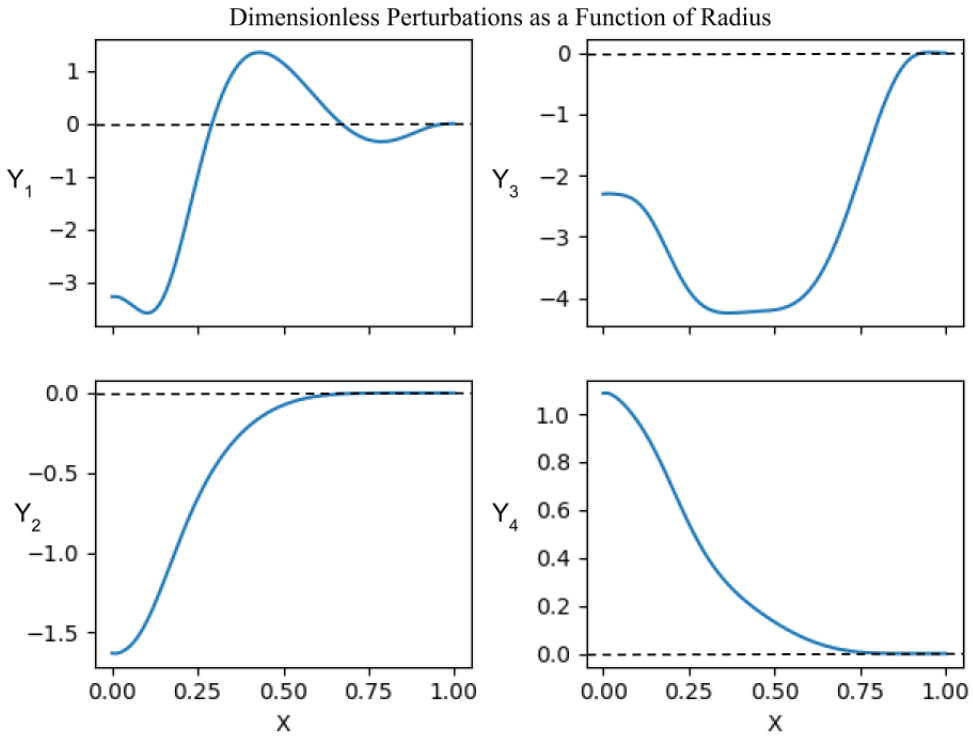

Figure 5: Dimensionless Perturbations as a function of radius for $l = 2$ 2^{nd} Harmonic Pressure-Mode for n=3 Polytrope. $x = 0$ is center of star, $x = 1$ is stellar surface

While the perturbation dynamics are interesting, the eigenfrequency the pulsation occurs at is generally more important, as it can be readily observed from Earth. The eigenfrequency for a Newtonian polytrope is solely a function of n among the equilibrium characteristics, and is also dependent on the spherical harmonic and particular mode.

Prior calculations by Christensen-Dalsgaard and Mullan have yielded the first few p-mode eigenfrequencies for $l = 1$, $l = 2$, and $l = 3$ to high precision [2]. I compared the results of our method, described in Section 1.3, against these literature values. As a sample, Table 1 below shows a comparison of our calculations against theirs for the first five eigenfrequencies of a star with polytropic index $n = 3$ and spherical harmonic degree $l = 2$.

Harmonic	Literature [2]	Calculated	Rel Error
Fundamental	3.90687	3.90687	$1.2491 * 10^{-7}$
2^{nd} Harmonic	5.169468	5.169469	$7.6588 * 10^{-8}$
3^{rd} Harmonic	6.439991	6.439990	$4.5185 * 10^{-8}$
4^{th} Harmonic	7.708951	7.708951	$1.8080 * 10^{-10}$
5^{th} Harmonic	8.975891	8.975891	$3.1879 * 10^{-8}$

Table 1: Dimensionless Frequencies of low harmonic pressure-modes ($l = 2$) for $n = 3$ Polytrope

With higher harmonics, the perturbation variables have a higher spatial frequency in the interior of the star, and have more zeroes and relative extrema. This makes numerically simulating these scenarios more complex, and less accurate than lower harmonics for equal number of integration steps. With increased integration steps, our model is sufficiently accurate even for higher harmonics. The below table uses the same polytropic equilibrium as Table 1, and the same spherical harmonic degree $l = 2$.

Harmonic	Literature [2]	Calculated	Rel Error
31^{st} Harmonic	41.5192	41.5221	$6.8743 * 10^{-5}$
32^{nd} Harmonic	42.7630	42.7664	$7.8022 * 10^{-5}$
33^{rd} Harmonic	44.0065	44.0104	$8.7698 * 10^{-5}$
34^{th} Harmonic	45.2497	45.2541	$9.7599 * 10^{-5}$
35^{th} Harmonic	46.4927	46.4977	$1.0758 * 10^{-4}$

Table 2: Dimensionless Frequencies of high harmonic pressure-modes ($l = 2$) for $n = 3$ Polytrope

Although the error in the higher harmonics is approximately 100 times larger in magnitude than the error in the first harmonics, it is still 1 part in $10,000$ or less. Given the strong match for both low and high eigenfrequencies, this code can be used to calculate frequencies for higher harmonics than previously reported ([2] goes to 50^{th}). However, these higher harmonics require greater energy, and thus occur at smaller amplitudes in real compact objects. Their study is useful for understanding patterns in stellar pulsations, but not for experimental asteroseismology.

6 Relativistic Quadrupole Oscillations

6.1 Perturbation Metric

Similar to in the Newtonian case, I use a polytropic model of the equilibrium structure. A perturbation is applied, and as a result of the motion, the geometry of spacetime around the relativistic star is no longer described by Equation (7). Rather, the new metric, involving the perturbation metric h_{uv}, becomes

$$ds^2 = (ds^2)_0 + h_{uv}dx^u dx^v \tag{21}$$

In even-parity Regge-Wheeler gauge, the perturbation metric takes the form [10]:

$$-h_{uv} = \begin{pmatrix} e^{\nu}\mu^l H_0 Y & i\omega(\mu^l H_1 Y) & 0 & 0 \\ i\omega(\mu^l H_1 Y) & e^{\lambda}(\mu^l H_0 Y) & 0 & 0 \\ 0 & 0 & r^2(\mu^l K Y) & 0 \\ 0 & 0 & 0 & r^2\sin^2(\theta)(\mu^l K Y) \end{pmatrix} \tag{22}$$

The variable μ is the dimensionless radius of the star (ranging from 0 to 1), $Y = e^{i\omega t} * Y_{lm}$ is the time dependence multiplied by the spherical harmonic of the perturbation. H_0, H_1, and K are functions of r only. The Regge-Wheeler gauge is preferred for only introducing two terms outside the main diagonal. Substituting into Equation (21), I obtain:

$$ds^2 = \begin{pmatrix} -e^{\nu}\big(1+\mu^l H_0 Y\big) & -i\omega(\mu^l H_1 Y) & 0 & 0 \\ -i\omega(\mu^l H_1 Y) & e^{\lambda}\big(1-\mu^l H_0 Y\big) & 0 & 0 \\ 0 & 0 & r^2\big(1-\mu^l K Y\big) & 0 \\ 0 & 0 & 0 & r^2\sin^2(\theta)\big(1-\mu^l K Y\big) \end{pmatrix} \tag{23}$$

6.2 Perturbations Inside the Compact Object

Inside the star, the perturbed fluid is described by a displacement ξ^{α}, where:

$$\xi^r = \frac{r^{l-1}}{e^{\lambda/2}} W * Y \tag{24}$$

$$\xi^{\theta} = -r^{l-2} V * \frac{\partial}{\partial\theta} Y \tag{25}$$

$$\xi^{\phi} = -\frac{r^{l-2}}{\sin^2(\theta)} V * \frac{\partial}{\partial\phi} Y \tag{26}$$

The three fluid perturbations have separable time- and radius-dependence, allowing for calculations done at a specified time to represent the system with the necessary transformations. The variables W and V are fluid perturbation variables that must be solved for to describe the nonradial stellar pulsations. Five variables are dependent on radius, H_0, H_1, K, W, and V. The first three relate to the initial spacetime perturbation, and W and V describe fluid perturbations [11].

Einstein's Field Equations can be applied to the spacetime metric given in Equation (23) to give differential equations for each perturbation variable. Using these relations, I can eliminate one variable, creating a system of four differential equations. Following Detweiler and Lindblom, H_1 is eliminated instead of H_0, to avoid possible singularities [12]. To simplify the resultant equations, X is defined as a function of W, V, and H_0:

$$X = \omega^2(\rho + p)e^{-\nu/2}V - r^{-1}\frac{dp}{dr}e^{(\nu-\lambda)/2}W + \frac{1}{2}(\rho + p)e^{\nu/2}H_0 \tag{27}$$

The four first-order differential equations for H_1, K, W, and X, are [12]:

$$\frac{dH_1}{dr} = -r^{-1}[l + 1 + 2Me^{\lambda}r^{-1} + 4\pi r^2 e^{\lambda}(p - \rho)]H_1 + r^{-1}e^{\lambda}[H_0 + K - 16\pi(p + \rho)V] \tag{28}$$

$$\frac{dK}{dr} = r^{-1}H_0 + \frac{1}{2}l(l + 1)r^{-1}H_1 - [(l + 1)r^{-1} - \frac{1}{2}\frac{d\nu}{dr}]K - 8\pi(p + \rho)e^{\lambda/2}r^{-1}W \tag{29}$$

$$\frac{dW}{dr} = -(l + 1)r^{-1}W + re^{\lambda/2}[\gamma^{-1}p^{-1}e^{-\nu/2}X - l(l + 1)r^{-2}V + \frac{1}{2}H_0 + K] \tag{30}$$

$$\frac{dX}{dr} = -(lr^{-1})X + (p + \rho)e^{\nu/2}\Bigg\{\frac{1}{2}\Big(r^{-1} - \frac{1}{2}\frac{d\nu}{dr}\Big)H_0 + \frac{1}{2}\Big[r\omega^2 e^{-\nu} + \frac{1}{2}l(l + 1)r^{-1}\Big]H_1 + \frac{1}{2}\Big(\frac{3}{2}\frac{d\nu}{dr} - r^{-1}\Big) - \frac{1}{2}l(l + 1)\frac{d\nu}{dr}r^{-2}V - r^{-1}\Big[4\pi(p + \rho)e^{\lambda/2} + \omega^2 e^{\lambda/2-\nu} - \frac{1}{2}r^2\frac{d}{dr}(r^{-2}e^{-\lambda/2}\frac{d\nu}{dr}\Big]W\Bigg\} \tag{31}$$

Equations (28) to (31) can be expressed in matrix form similar to Equation (14), and are handled computationally in this manner. A major difference between the Newtonian and relativistic calculations is that the relativistic calculations are dimensioned while Newtonian is dimensionless. Only two of the four linearly independent solutions to this system are well-behaved at the center of the star (at $r = 0$). The perturbed pressure must vanish at $r = R$, so $X(R) = 0$. From these conditions, a single acceptable solution is specified for each frequency ω.

At the central boundary, $r = 0$, the differential equations are singular, as they contain multiple $1/r$ terms that tend the function to infinity. Since the numerical integration cannot be started at $r = 0$, a power-series approximation is used to determine an appropriate starting condition slightly away from the center, following the procedure described in [11] and [12]. These equations are the most complex of the entire algorithm, but critical to accurately model the stellar oscillations at the center of the compact object.

The power series approximations are used to $r = 0.01R$. Then, the differential equations are integrated using fourth-order Runge-Kutta integration to $r = 0.5R$. There are two linearly independent solutions, labelled Y_1 and Y_2. Similarly, the three solutions from the exterior of the star are iterated to the midpoint of the interval, giving Y_3, Y_4, and Y_5. A linear combination of these five solutions exists that makes each variable H_1, K, W, and X continuous at the midpoint. With five solutions for four variables, there is an extra degree of freedom. This additional degree allows for free-scaling of the solution.

6.3 Perturbations Outside the Compact Object

Given any spherical harmonic degree and frequency, I can find the unique solution for the radial dependent variables H_1, K, W, and X that define the perturbations in the interior of the star. I are mainly interested in solutions composed only of outgoing waves, as these represent resonant oscillation and the energy radiated from the star. These frequencies are called Quasi-Normal Modes (QNMs), and include the relativistic-equivalent of Newtonian p-modes.

To find these specific eigenfrequencies, I analyze the perturbation variables outside the compact object to determine the gravitational radiation produced. In the exterior of the star, the fluid perturbations W, V, and X are zero and the two metric perturbations H_1 and K can be combined to obtain the single second-order differential equation known as the Zerilli equation [13].

$$\left[\frac{d^2}{dr_*^2} + \omega^2 - V_Z(r)\right] Z = 0 \tag{32}$$

With the effective potential V_Z given by:

$$V_Z(r) = 2\Big(1 - \frac{2M}{r}\Big) * \frac{n^2(n+1)r^3 + 3n^2Mr^2 + 9nM^2r + 9M^3}{r^3(nr+3M)^2} \tag{33}$$

The tortoise coordinate r_* is defined by:

$$\frac{d}{dr_*} = \Big(1 - \frac{2M}{r}\Big)\frac{d}{dr} \tag{34}$$

The Zerilli equation is notable because it provides a Schrödinger-type equation for even-parity Regge-Wheeler perturbations of Schwarzschild geometry. This presents simplifications to the analysis of wave equations [14]. The Zerilli function is defined in terms of the metric perturbations $H_0(r)$ and $K(r)$

$$\begin{bmatrix} 0 & 1 \\ a(r) & b(r) \end{bmatrix} \begin{bmatrix} H_0(r) \\ K(r) \end{bmatrix} = \begin{bmatrix} g(r) & 1 \\ h(r) & k(r) \end{bmatrix} \begin{bmatrix} Z(r_*) \\ dZ(r_*)/dr_* \end{bmatrix} \tag{35}$$

Where the functions $a(r)$, $b(r)$, $g(r)$, $h(r)$, and $k(r)$ are functions of the frequency, spherical harmonic degree, and mass and radius of the compact object, given in [11]. I recover H_0 with the following equation, similar to the relation defined between V and X in Equation (27).

$$\left[3M + nr - 4\pi r^3\rho\right] H_0 = \left[\omega^2 r^3 e^{-\lambda-\nu} - \frac{l(l+1)}{2}(M + 4\pi r^3 p)\right] H_1 - \left[\omega^2 r^3 e^{-\nu} - nr - M - 4\pi r^3 p - \frac{e^{\lambda}}{r}(M + 4\pi r^3 p)^2\right] K \tag{36}$$

Using Equation (35), I obtain initial conditions for $Z(r_*)$ and $dZ(r_*)/dr_*$. For a given (r_*, Z) coordinate, Equation (32) can be used to calculate d^2Z/dr_*^2, and in this manner I propagate Z through r_*. In practice, I integrate Z from $r_* = R_*$ to $r_* = 25\omega^{-1}$ [11]. Far away from the star, the Zerilli function can be expressed as a combination of two components, namely the ingoing and outgoing contributions. These individual solutions may be asymptotically expressed as power series.

$$Z_-(r_*) = e^{i\omega r_*} \sum_{j=0}^{\infty} a_j r^{-j} \tag{37}$$

$$Z_+(r_*) = e^{i\omega r_*} \sum_{j=0}^{\infty} \bar{a}_j r^{-j} \tag{38}$$

The solution Z_- represents purely outgoing gravitational radiation, while Z_+ represents purely ingoing waves. The constants a_j and the complex conjugates $\bar{a}_j$ are recursively defined in [15]. A solution to the Zerilli equation will be given by a constant linear combination of Z_+ and Z_-.

$$Z(r_*) = \beta(\omega) Z_-(r_*) + \gamma(\omega) Z_+(r_*) \tag{39}$$

For Quasi-Normal Modes, all the gravitational radiation is outgoing, so the particular solution Z should be a multiple of Z_-, with no parts Z_+. At $r = 25\omega^{-1}$, the Zerilli equation numerically integrated is matched onto the asymptotic series, with $j_{max} = 2$. I determine values of constants $\beta(\omega)$ and $\gamma(\omega)$, and use Newton's method to search for ω such that $\gamma(\omega) = 0$. The eigenfrequencies found are those of quasinormal modes, a subset of which correspond to the Newtonian Pressure-Modes.

$$\Delta\ \omega = \omega_R - \omega_N \tag{40}$$

I compare the difference in frequencies of these corresponding modes Equation (40) against the relativity parameter σ defined in Equation (6) to understand the effects of general relativity on pulsation frequencies of compact objects, the ultimate goal of this research.

6.4 Algorithmic Roadmap

A similar approach is taken here compared to the Newtonian model (See Section 4.2). However, there are some key differences in the implementation. Instead of using the Lane-Emden Equation, the Tolman-Oppenheimer Equation is used (Eq. 8-10). After integrating the Equations (28)-(31) in the interior of the star, the Zerilli function and its derivatives are computed at $r = R$ (Eq. 32-36). Runge-Kutta integration is used to iterate the Zerilli function far from the star where it is matched onto the asymptotic power-series expansions and the coefficients $\beta(\omega)$ and $\gamma(\omega)$ are calculated (Eq. 39). $\gamma(\omega)$ replaces $\det(M)$ in the Newtonian model, and I proceed as before locating eigenfrequencies for various spherical harmonics.

7 Relativistic Model Results and Discussion

The figure below shows the normalized perturbations of a polytrope with $n = 3$ as a function of dimensionless radius r. Although $n = 1$ is most optimal for a neutron star, I use $n = 3$ initially to best compare to the Newtonian model. The spherical harmonic degree is $l = 2$, and this particular perturbation is the second harmonic pressure mode. The four graphs left to right and top to bottom are perturbation variables X, W, K, and X_0. Recall K and X_0 represent metric perturbations (Eq. 23). The shape of these curves closely match the shapes of y_3 and y_4 in the Newtonian section (Figure 5). X and W are different variables than y_1 and y_2, explaining the differences in the shapes of the top two panels between Figure 5 and 6.

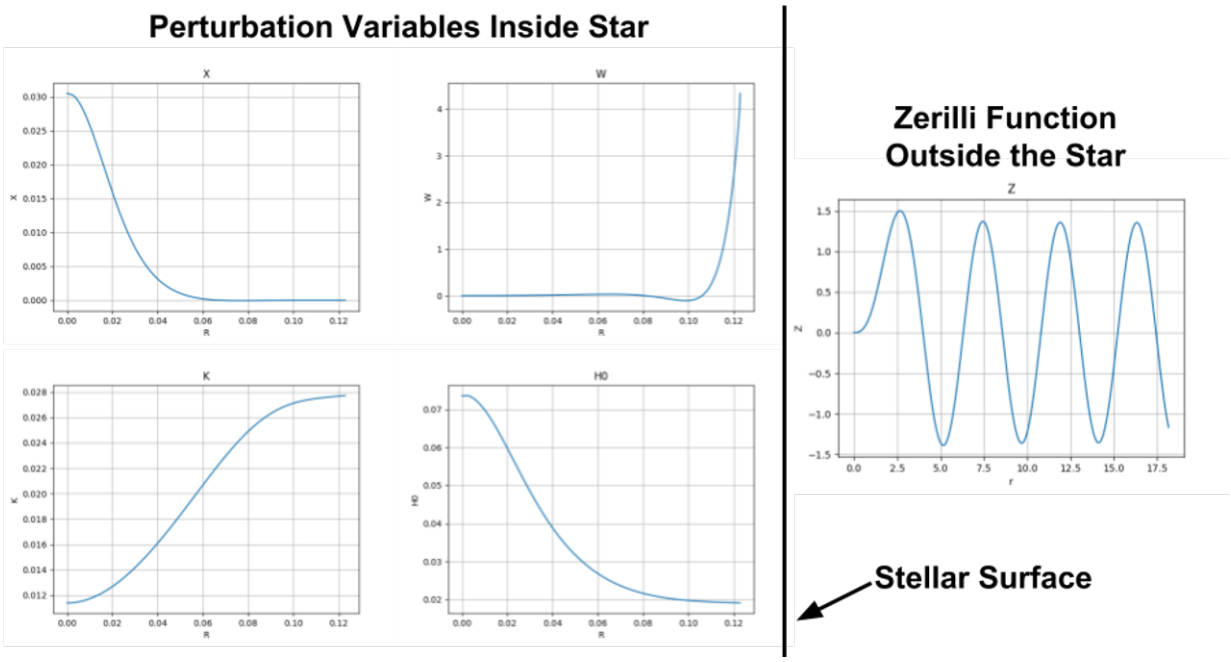

Figure 6: Perturbation variables calculated for a specific pulsation, with corresponding Zerilli variable integrated outside the compact object using the Zerilli equation

These results are a strong indication that the integration inside of the star is accurate, and successfully predicting the shape of the interior perturbation variables. The left panel in Figure 6 shows the Zerilli function through dimensionless radius, solved using the Zerilli equation. The single discernible frequency and sinusoidal shape indicates these calculations are accurate as well. I am still working on searching for quasinormal modes using Newton's Method. Until then, I cannot compare the frequencies of the Newtonian and Relativistic models. However, these figures do show that the Relativistic model functions very similarly to the Newtonian model, with differences generally in value while maintaining the perturbation variables through radius.

References

[1] Bowman, D. M., Buysschaert, B., Neiner, C., Pápics, P. I., Oksala, M. E., and Aerts, C. K2 space photometry reveals rotational modulation and stellar pulsations in chemically peculiar a and b stars. *A&A*, 616:A77, 2018.

[2] J. Christensen-Dalsgaard and D. J. Mullan. Accurate frequencies of polytropic models. *Royal Astronomical Society*, 1993.

[3] M. E. Caplan, A. S. Schneider, and C. J. Horowitz. Elasticity of nuclear pasta. *Phys. Rev. Lett.*, 121:132701, Sep 2018.

[4] Jill Knapp. Polytropes. 2011.

[5] J. B. Hartle. *Gravity: An introduction to Einstein's general relativity.* Addison-Wesley, San Francisco, 1 edition, 2003.

[6] R. F. Tooper. General relativistic polytropic fluid spheres. *The Astrophysical Journal*, 140(434), 1964.

[7] Wikimedia Commons. CC-BY-SA-3.0. GFDL Tosaka.

[8] W. Unno. *Nonradial oscillations of stars.* University of Tokyo Press, Tokyo, 2 edition, 1989.

[9] R. Townsend and S. Teitler. Gyre: An open-source stellar oscillation code based on a new magnus multiple shooting scheme. 2013.

[10] K. S. Thorne and A. Campolattaro. Non-radial pulsation of general-relativistic stellar models. i. analytic analysis for $l \geq 2$. *The Astrophysical Journal*, 149:591, Sep 1967.

[11] L. Lindblom and S. L. Detweiler. The quadrupole oscillations of neutron stars. *The Astrophysical Journal*, 1983.

[12] L. Lindblom and S. L. Detweiler. On the nonradial pulsations of general relativistic stellar models. *The Astrophysical Journal*, 1985.

[13] K. D. Kokkotas N. Andersson and B. F. Shutz. A new numerical approach to the oscillation modes of relativistic stars. 1995.

[14] E. D. Fackerell. Solutions of zerilli's equation for even-parity gravitational perturbations. *The Astrophysical Journal*, 1971.

[15] S. Chandrasekhar and S. Detweiler. The quasi-normal modes of the schwarzschild black hole. *The Royal Society*, 1975.